Strong Field Multiphoton Inversion of a Three-Level System Using Shaped Ultrafast Laser Pulses

Stephen D. Clow,[1] Carlos Trallero-Herrero,[2] Thomas Bergeman,[1] and Thomas Weinacht[1]
[1]*Department of Physics Stony Brook University, Stony Brook, New York 11794, USA*
[2]*National Research Council of Canada, 100 Sussex Drive, Ottawa, Ontario K1A 0R6, Canada*
(Received 4 October 2007; revised manuscript received 13 December 2007; published 12 June 2008)

We demonstrate strong-field population inversion in a three-level system with single and multiphoton coupling between levels using a single shaped ultrafast laser pulse. Our interpretation of the pulse shape dependence illustrates the difference between sequential population transfer and adiabatic rapid passage in three-level systems with multiphoton coupling between levels.

DOI: 10.1103/PhysRevLett.100.233603 PACS numbers: 42.50.Hz

There is significant interest in controlling atomic and molecular dynamics using shaped laser pulses [1–7]. An important aspect of this is selectively populating a particular target state with high efficiency. Many techniques have been developed that make use of strong-field coupling to atomic or molecular states via single-photon (dipole allowed) transitions. These include adiabatic rapid passage and variants—chirped adiabatic rapid passage [8,9] and stimulated raman adiabatic passage (STIRAP) [10]. While these approaches are powerful and effective, there is also interest in extending them to multiphoton coupling between atomic and molecular levels [11–14]. In order to achieve efficient population transfer beyond the limits of single-photon excitation, one must consider nonlinear coupling between states, multiple interfering pathways and dynamic Stark shifts (DSS), which make resonance conditions time dependent and substantially modify the phase advance of the bare states during the atom- or molecule-field interaction. A dramatic example of this is the transition from stimulated absorption to stimulated emission well before half a Rabi cycle is complete in strong-field two-photon absorption [15,16].

Here, we demonstrate a population inversion via three-photon absorption using a strong-field shaped ultrafast laser pulse. Typically, the population in an excited state is inferred based on numerical integration of the Schrödinger equation. Here we measure the excited state population through a combination of stimulated and spontaneous emission. A genetic algorithm (GA) inside a control loop is used to discover optimal pulse shapes for the population transfer [17], and we interpret the dynamics underlying the atom-field interaction via pulse shape parameter scans based on the measured optimal pulse shapes and numerical integration of the Schrödinger equation. Our interpretation of the dynamics highlights the difference between single-photon and multiphoton coupled adiabatic rapid passage. The experiments are carried out in atomic sodium [15,18–20], where $7p$ is the target state. The $3s$ ground state is two-photon resonant with the $4s$ state at 777 nm, and the $4s$-$7p$ transition is resonant at 781 nm.

Our laser system produces $\approx$ 1 mJ 30 fs pulses, tunable from 772 nm to 784 nm. They are shaped in an acousto-optic modulator based pulse shaper and directed into a heat pipe oven containing sodium vapor with an argon buffer gas at approximately 270 °C. Both fluorescence and stimulated emission are collected from the excited atoms. Fluorescence from the center of the heat pipe oven was collected at 90° with respect to the beam propagation direction with an $f2$ lens and imaged onto a photomultiplier tube. We image a spatially filtered focus into the heat pipe oven to avoid intensity averaging [21].

Atoms initially excited to the $7p$ state undergo inelastic collisions with argon atoms in the heat pipe oven on time scales much faster than the $7p$ natural lifetime. We therefore measured fluorescence from the $7s$-$3p$, $6d$-$3p$, $4d$-$3p$, $6s$-$3p$, and $5s$-$3p$ transitions. Comparing the sum of these fluorescence channels from the $7p$ state with fluorescence on the $3p$-$3s$ line, which is produced from both $7p$ and $4s$ atoms, allowed us to determine the fraction of excited atoms that were initially excited to the $7p$ state. Measurements of superfluorescence on the $3p$-$3s$ transition for a pulse that excites the $4s$ state allowed us to determine the fraction of atoms excited above the ground state ($4s$ and $7p$), since earlier work demonstrated a sharp threshold in the $4s$ state population (0.66) for superfluorescence to occur [22]. Combining these two measurements therefore allowed us to determine the population of the $7p$ state (before collisions) without having to rely on knowledge of the density of atoms in the focus, the solid angle subtended by the detector, or our absolute detection efficiency. The details are given in a separate publication [23].

In order to discover an optimal pulse shape for populating the $7p$ state, we used the $7s$-$3p$ and $6d$-$3p$ fluorescence [24] as a feedback signal for our GA. The fluorescence for a shaped and an unshaped pulse is shown in Fig. 1 and illustrates an order of magnitude gain in the population transfer with pulse shaping. The inset shows the Wigner distribution for an optimally shaped pulse discovered by our GA. Table I summarizes our measurements of the $7p$ population for an optimized laser pulse.

The Wigner distributions for different GA runs showed varying temporal structure, but many showed clear indications of a negative linear chirp as shown in Fig. 1. This motivated the experimental and numerical study of popu-

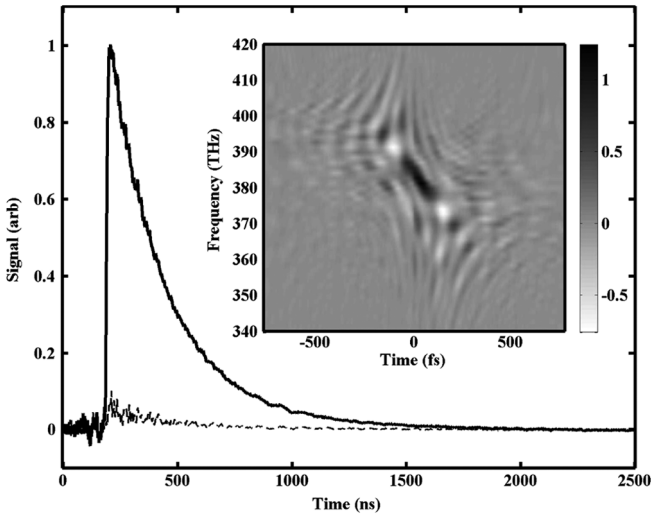

FIG. 1. The solid and dashed curves show fluorescence measurements (including light from the $7s$-$3p$ and $6d$-$3p$ transitions) for GA optimized and unshaped laser pulses; the inset shows the Wigner distribution for an optimal pulse.

lation transfer as a function of linear chirp or quadratic spectral phase. We numerically integrated the Schrödinger equation and measured the fluorescence yield as functions of intensity and chirp. Working in the rotating wave approximation and adiabatically eliminating nonresonant atomic levels [15,21,25], we can express the time-dependent atom-field Hamiltonian in the interaction picture as

$$\hat{\mathbf{H}}_{\mathbf{I}}(t) = \begin{pmatrix} \omega_g^{(s)}(t) + \Delta(t) & \chi^*(t) & 0 \\ \chi(t) & \omega_e^{(s)}(t) & \chi_{er}^*(t) \\ 0 & \chi_{er}(t) & \omega_r^{(s)}(t) - \Delta_{er}(t) \end{pmatrix}. \tag{1}$$

Here $\Delta(t) = \Delta_0 - \frac{\beta t}{2(1/\tau^4+\beta^2)}$ and $\Delta_{er}(t) = (\Delta_{er})_0 - \frac{\beta t}{4(1/\tau^4+\beta^2)}$, Δ_0 and $(\Delta_{er})_0$ are the two and one-photon atom-field detunings, τ is the pulse duration for an unshaped pulse, β is the frequency domain chirp rate, $\omega_g^{(s)}(t)$, $\omega_e^{(s)}(t)$, and $\omega_r^{(s)}(t)$ represent the time-varying DSS of the ground, excited, and resonant ($7p$) states, respectively, $\chi(t)$ represents the two-photon Rabi frequency, μ_{re} is the one-photon coupling between the excited and resonant states ($4s$ and $7p$), $\varepsilon(t)$ is the electric field, and $\chi_{er}(t) = \frac{\mu_{re}}{2\hbar}\varepsilon(t)$.

TABLE I. Measured fraction of excited atoms, fraction of atoms in the $7p$ state, and $7p$ population with corresponding standard deviation (STD). The values correspond to an average of 5 different GA trials at a fixed temperature of 270 °C and central wavelength of 778 nm.

	$\lvert\Psi_{4s}\rvert^2 + \lvert\Psi_{7p}\rvert^2$	$\lvert\Psi_{7p}\rvert^2/(\lvert\Psi_{4s}\rvert^2 + \lvert\Psi_{7p}\rvert^2)$	$\lvert\Psi_{7p}\rvert^2$
Value	0.69	0.89	0.61
STD	0.09	0.08	0.09

The calculation results shown in Fig. 2(b) agree with the measurements in Fig. 2(a). U_0 is the minimum pulse energy for a pi pulse on the $3s$-$4s$ transition, which corresponds to ≈ 12 μJ for a 50 fs pulse with a uniform intensity profile in our focal geometry. We note a strong asymmetry in population transfer to the $7p$ state, with a high yield for negative chirp and a low yield for positive chirp. The white X in Fig. 2(a) corresponds to the quadratic phase of the optimal pulse discovered by the GA. Calculations for the population transfer without the DSS show much larger population transfers for positive chirp (roughly a factor of 4 higher than with the DSS). The intuitive ordering of frequencies in the pulse, where first the atoms are driven from the $3s$ to the $4s$ state (two-photon resonant at 777 nm and Stark shifted to the higher frequency) with the blue frequency components and then from the $4s$ to the $7p$ state (resonant at 781 nm) with the red components is effective. However, in contrast to measurements of population transfer with single-photon excitation of the intermediate state [11], the counterintuitive ordering of frequencies (as in STIRAP) is not effective in our situation. This contrast motivates us to examine the underlying dynamics in more detail.

Figure 3 shows calculated populations of the $3s$, $4s$, and $7p$ states as a function of time for pulses with a fixed energy of $3U_0$ and chirp rates of -0.002 ps^2 [3(c)] and 0.002 ps^2 [3(d)]. Figures 3(a) and 3(b) show Wigner distributions for pulses with chirp rates of (a) -0.002 ps^2 and

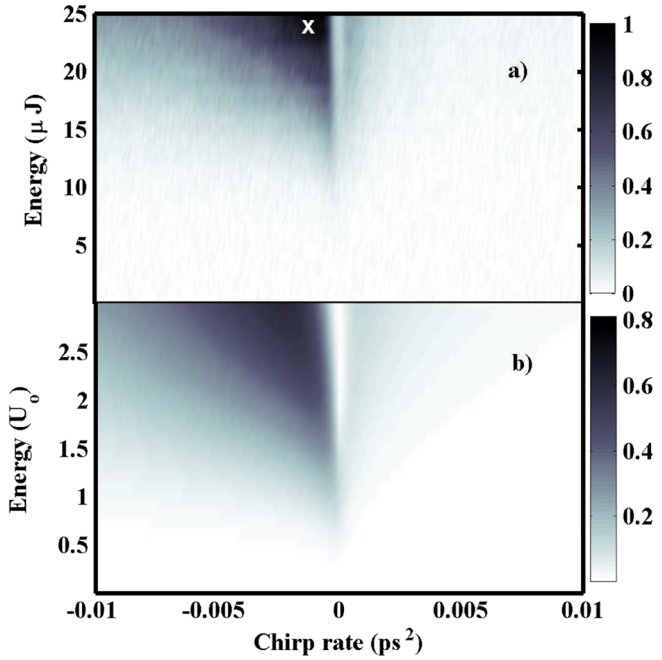

FIG. 2 (color online). (a) Measurement of $7s$-$3p$ and $6d$-$3p$ fluorescence as a function of chirp. The data are normalized to the maximum fluorescence measured and the white X marks the chirp rate associated with a pulse discovered by the GA. (b) Simulation of the $7p$ population as a function of pulse energy and chirp.

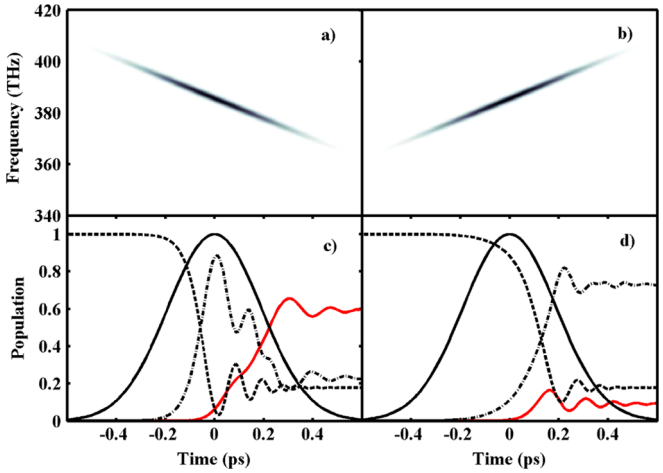

FIG. 3 (color online). Calculated Wigner distributions for chirp rates of (a) -0.002 ps^2 and (b) 0.002 ps^2. (c),(d) The $3s$ (dashed line), $4s$ (dash-dotted line), and $7p$ (solid red line) populations, as well as the field envelope (solid black line), corresponding to (a) and (b), respectively, for a pulse energy of $3U_0$.

(b) 0.002 ps^2. For a negative chirp, the pulse starts blue detuned relative to the bare $3s$-$4s$ transition frequency and is able to efficiently drive population from the $3s$ to the $4s$ state on the rising edge of the pulse since a blue detuning can compensate for the average dynamic Stark shift on this transition [16]. Then as the frequency of the pulse sweeps to the red at high intensity, Rabi oscillations off resonance (coherent transients [7]) drive population between the $3s$ and $4s$ states with decreasing amplitude. Finally, as the frequency of the pulse sweeps through resonance for the $4s$-$7p$ transition, population is transferred to the $7p$ state resulting in a population inversion. The final $7p$ population is about ≈ 0.6. However, the opposite chirp, shown in 3(b), yields a different behavior. Here, the pulse starts out closer to resonance with the $4s$-$7p$ transition, but far off resonance with the $3s$-$4s$ transition. As the intensity increases, the separation between the $3s$ and $4s$ states increases with the DSS, keeping these states out of resonance despite the increasing instantaneous frequency of the pulse. Once the pulse intensity reaches its peak and starts to decrease, with the instantaneous frequency still increasing, the pulse can sweep through resonance on the $3s$-$4s$ transition, transferring population to the $4s$ state. Now the frequency is far detuned from the $4s$-$7p$ transition frequency and the intensity is sufficiently low that there is ineffective transfer to the $7p$. Rather than driving population from the $3s$ to the $7p$ state without going through the $4s$ (as one might expect if STIRAP were effective here), significant population is driven to the $4s$ state, and there is marginal transfer to the $7p$ state (≈ 0.09).

A dressed state analysis illustrates a key problem associated with adiabatic passage involving multiphoton coupling. Not only are the shape of the dressed states influenced unfavorably by the DSS (the avoided crossings become smaller), but more importantly, the spacing between avoided crossings scales differently with the intensity for single vs multiphoton coupling between levels, making the nonadiabatic corrections large for all chirp values at our pulse energies. Figure 4 shows the dressed states as a function of central wavelength for an intensity of 1.44×10^{15} W/m^2.

Analytic calculations of the nonadiabatic corrections to STIRAP are complicated by two features of our Hamiltonian: the detunings between the two pairs of states are not the same, and dynamic Stark shifts are on the diagonal entries of the Hamiltonian [25]. Therefore, we have calculated the nonadiabatic corrections to adiabatic passage numerically as a function of spectral chirp rate, β. This is the most natural pulse shape parameter to vary as it directly controls the time-dependent detunings $\Delta(t)$ and $\Delta_{er}(t)$, and can be easily controlled at a fixed pulse energy. Our calculations compare the difference between the eigenvalues for the total effective interaction Hamiltonian and the adiabatic Hamiltonian normalized by the eigenvalues for the adiabatic Hamiltonian. This is a direct measure of adiabaticity [25]—when this ratio is much smaller than 1, then the passage can be adiabatic, but when the difference is large, then population can cross between dressed states and adiabaticity is lost.

If $\mathbf{U}(t)$ is the matrix that diagonalizes $\mathbf{H_I}(t)$:$\mathbf{D(t)} = \mathbf{U(t)}^{-1}\mathbf{H_I(t)U(t)}$, then the evolution of the dressed states is given by the total effective interaction Hamiltonian: $\mathbf{H_I'} = \mathbf{D} - i\mathbf{U}^{-1}\dot{\mathbf{U}}$, where $\mathbf{D}$ is a diagonal matrix with the dressed state energies as the diagonal elements. We computed the eigenvalues of $\mathbf{H_I'}$ and $\mathbf{D}$, and then divided their difference by the eigenvalues of $\mathbf{D}$ as a function of the frequency domain chirp parameter, β. Intuitively, one might expect the nonadiabatic corrections to decrease with increasing values of β since for $\beta \gg 1/\tau^2$, $|\dot{\Delta}(t)| \sim \frac{1}{\beta}$, and the passage is more adiabatic for smaller $|\dot{\Delta}(t)|$.

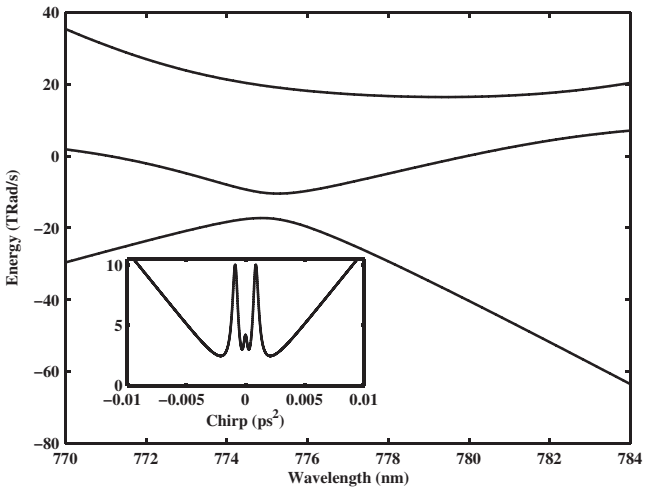

FIG. 4. Calculated dressed states using $\mathbf{H_I}(t)$. The inset shows normalized nonadiabatic corrections for one of the eigenvalues of equation $\mathbf{H_I'}(t)$ as a function of β.

However, increasing β also decreases the peak electric field of the pulse. As the splitting between dressed states scales nonlinearly with the field for multiphoton coupling ($\chi \sim \varepsilon^2$ in our case), increasing β can actually increase the importance of the nonadiabatic corrections to the eigenvalues and make the passage less adiabatic. The criterion for adiabatic passage with single-photon coupling, a single detuning, and a slowly varying envelope is usually given by $\frac{|\dot{\Delta}(t)|}{\chi^2(t)+\Delta^2(t)} \ll 1$ [25]. In our case, since $|\dot{\Delta}(t)| \sim 1/\beta$ and $\chi \sim 1/\beta$, it is clear by this criterion (for $\Delta = 0$) that increasing β makes the passage less adiabatic despite the fact that the frequency sweep is slower. Our numerical calculations of the nonadiabatic corrections, shown in Fig. 4, illustrate this point for our Hamiltonian. The structure in the graph for low β is a result of the fact that we are showing the variation with β (as this is the experimentally relevant parameter), while it is $\dot{\Delta}(t)$, which determines the frequency sweep in time and $\Delta(t) = \Delta_0 - \frac{\beta t}{2(1/\tau^4+\beta^2)}$. For $\beta \gg 1/\tau^2$ it is clear that increasing β leads to larger nonadiabatic corrections, as one expects from the reasoning above. Adiabatic passage for a chirped ultrafast laser pulse would require pulse energies 1 to 2 orders of magnitude higher than we have used in our experiments. For the optimal β value shown in the graph ($\sim$0.002), an increase in pulse energy by an order of magnitude would still leave nonadiabatic corrections of about 30%. Increasing the pulse energy by over an order of magnitude at this β value would lead to peak intensities higher than for an unshaped laser pulse, and ionization would no longer be negligible. Therefore, we argue that sequential population transfer is inherently more effective than adiabatic passage when using shaped ultrafast lasers to drive population transfer in a multilevel system using multiphoton coupling between levels.

In conclusion, we demonstrate strong-field multiphoton inversion of a three-level atomic system using a single shaped ultrafast laser pulse. Shaping yields an order of magnitude gain over the population transfer for a unshaped laser pulse. We interpret the physical mechanism underlying control by performing parametrized pulse shape scans based on the optimal pulses and numerical integration of the Shrödinger equation. The pulse shape dependence of the final state population illustrates the benefits of sequential vs STIRAP-like population transfer for a fixed pulse energy. In the case of multiphoton population transfer with a single ultrafast laser pulse, there are no decoherence mechanisms on the time scales of the atom-field interaction and thus no disadvantage to populating intermediate states. Furthermore, the scaling of the adiabaticity criterion for STIRAP with multiphoton coupling is unfavorable and requires orders of magnitude higher pulse energies than sequential population transfer. Thus, we propose that sequential population transfer through intermediate states can be more effective than STIRAP based schemes when using shaped ultrafast laser pulses for population transfer with multiphoton coupling.

This work was supported by the National Science Foundation under Grant No. 0555214.

[1] N. Dudovich, B. Dayan, S. M. Gallagher-Faeder, and Y. Silberberg, Phys. Rev. Lett. **86**, 47 (2001).
[2] H. Rabitz, R. de Vivie-Riedle, M. Motzkus, and K. Kompa, Science **288**, 824 (2000).
[3] R. Bartels, S. Backus, E. Zeek, L. Misoguti, G. Vdovin, I. P. Christov, M. M. Murnane, and H. C. Kapteyn, Nature (London) **406**, 164 (2000).
[4] B. J. Sussman, M. Y. Ivanov, and A. Stolow, Phys. Rev. A **71**, 051401 (2005).
[5] A. Assion, T. Baumert, M. Bergt, T. Brixner, B. Kiefer, V. Seyfried, M. Strehle, and G. Gerber, Science **282**, 919 (1998).
[6] M. Wollenhaupt, A. Prakelt, C. Sarpe-Tudoran, D. Liese, and T. Baumert, J. Opt. B **7**, S270 (2005).
[7] A. Monmayrant, B. Chatel, and B. Girard, Phys. Rev. Lett. **96**, 103002 (2006).
[8] B. Broers, H. van Linden van den Heuvell, and L. Noordam, Phys. Rev. Lett. **69**, 2062 (1992).
[9] S. Chelkowski, A. Bandrauk, and P. Corkum, Phys. Rev. Lett. **65**, 2355 (1990).
[10] K. Bergmann, H. Theuer, and B. Shore, Rev. Mod. Phys. **70**, 1003 (1998).
[11] D. Goswami, Phys. Rep. **374**, 385 (2003).
[12] N. Dudovich, T. Polack, A. Pe'er, and Y. Silberberg, Phys. Rev. Lett. **94**, 083002 (2005).
[13] A. Rangelov, N. Vitanov, L. Yatsenko, B. Shore, T. Halfmann, and K. Bergmann, Phys. Rev. A **72**, 053403 (2005).
[14] G. N. Gibson, Phys. Rev. A **72**, 041404(R) (2005).
[15] C. Trallero-Herrero, J. Cohen, and T. C. Weinacht, Phys. Rev. Lett. **96**, 063603 (2006).
[16] C. Trallero-Herrero, D. Cardoza, T. C. Weinacht, and J. L. Cohen, Phys. Rev. A **71**, 013423 (2005).
[17] R. Judson and H. Rabitz, Phys. Rev. Lett. **68**, 1500 (1992).
[18] A. Präkelt, M. Wollenhaupt, C. Sarpe-Tudoran, and T. Baumert, Phys. Rev. A **70**, 063407 (2004).
[19] A. Gandman, L. Chuntonov, L. Rybak, and Z. Amitay, Phys. Rev. A **75**, 031401 (2007).
[20] R. R. Jones, Phys. Rev. Lett. **74**, 1091 (1995).
[21] C. Trallero-Herrero and T. C. Weinacht, Phys. Rev. A **75**, 063401 (2007).
[22] C. Trallero-Herrero, M. Spanner, and T. C. Weinacht, Phys. Rev. A **74**, 051403 (2006).
[23] C. Trallero-Herrero, S. D. Clow, T. Bergeman, and T. Weinacht, J. Phys. B **41**, 074014 (2008).
[24] Y. Ralchenko, F. C. Jou, D. E. Kelleher, A. E. Kramida, A. Musgrove, J. Reader, W. L. Wiese, and K. Olsen, in *NIST Atomic Spectra Database, NIST Standard Reference Database Number 78* (National Institute of Standards and Technology, Gaithersburg, MD 20899, 2006), http://physics.nist.gov/PhysRefData/ASD/.
[25] D. J. Tannor, *Introduction to Quantum Mechanics: A Time-dependent Perspective* (University Science Books, Sausalito, California, 2007).